Desalination and Water Treatment
www.deswater.com
doi: 10.5004/dwt.2022.28648

266 (2022) 163–172
August

The treatment of Pb(II) ions in wastewater by electrosorption

Fang Li*, Zhengwen Lin, Huanqing Zhai, Xinyu Liu

School of Petroleum and Gas Engineering, Southwest Petroleum University, Chengdu 610500, China, emails: mclifang@163.com (F. Li), scholarlin@qq.com (Z. Lin), 1413823645@qq.com (H. Zhai), 1263181543@qq.com (X. Liu)

Received 12 February 2022; Accepted 10 June 2022

ABSTRACT

Graphene oxide was successfully synthesized by the modified Hummers method using graphite as the raw material, and characterized by X-ray diffraction, Fourier-transform infrared spectroscopy and scanning electron microscopy. In this study, graphene oxide was used as the electrode for the removal of Pb(II) ions by electrosorption. The effects of adsorption time, voltage, pole plate spacing and initial Pb(II) ions concentration on the electrosorption were investigated. The experimental results showed that the adsorption efficiency of Pb(II) ions was significantly improved, and the optimum conditions for adsorption at the graphene oxide electrode were the adsorption time of 60 min, the adsorption voltage of 30 V and the pole plate spacing of 0.5 cm. The electrode adsorption under these conditions was 627.02 mg/g and the Pb(II) ions removal efficiency was 63.3%. By applying a reverse voltage to the electrode, the experimental electrode regeneration performance of the graphene oxide electrode was investigated. The experimental results showed that the regeneration performance of the graphene oxide electrode was good and stable, and the regeneration efficiency of the electrode was maintained at about 72% after six adsorption regeneration cycles.

Keywords: Graphene oxide; Pb(II) ions; Electrosorption; Electrode regeneration

1. Introduction

Heavy metals widely exist in wastewater, which can cause damage to the ecological environment and harm to humans [1,2]. Among them, Pb(II) ions not only damage human brain cells, nerve function and kidney function, but also cause dementia and brain death in the elderly [3,4]. In order to reduce the hazards of heavy metal pollution, there has been a lot of research on Pb(II) ions treatment at home and abroad. At present, the main treatment methods include chemical precipitation, ion-exchange, electrochemical and adsorption methods [5,6]. The most widely used method is adsorption method, but this method is limited by factors such as the adsorption capacity of the adsorbent, the limited adsorption rate, and the high regeneration cost [7–9]. Electrosorption is an emerging electrochemical desalination technology with the advantages of high energy efficiency, low environmental impact and low cost [10–13]. The removal of Pb(II) ions is achieved by applying a voltage to the working electrode, so that Pb(II) ions are adsorbed to the electrode surface under the action of electric field force [14]. Electrosorption can further increase the adsorption capacity of the material, and regenerate the electrode by applying a reverse voltage to desorb the Pb(II) ions, thus enabling the electrode to be recycled [15–17].

Graphene oxide is a new type of two-dimensional carbon nanomaterial with a large number of oxygen-containing groups such as hydroxyl, carboxyl and epoxy groups on its surface [18,19]. Graphene oxide is a promising material for electrosorption electrode due to its large specific surface area, good electrical conductivity and stable chemical properties [20–22]. There are three main traditional methods for the preparation of graphene oxide: the Brodie, Standenmaier and Hummers methods [23]. Compared with the other two methods, the Hummers method is the most commonly used method for the preparation of graphene oxide due to

* Corresponding author.

its short reaction time, high safety and low environmental pollution. The graphene oxide prepared by the modified Hummers method has the advantages of abundant oxygen-containing functional groups and low carbon layer destruction, which enhance its adsorption of heavy metal ions [24]. Most of the graphene oxide prepared by the modified Hummers method also differ to some extent due to the amount of oxidant and oxidation time.

In this study, graphene oxide (GO) was synthesized by the modified Hummers method, specifically by increasing the amount of oxidant $KMnO_4$ and increasing the low temperature oxidation time, and then exfoliating the GOs into layered graphene oxide by ultrasonication. The structure and properties of the synthesized graphite oxide were characterized, and electrosorption experiments were carried out with graphene oxide as the electrode plate material. The effects of time, voltage, electrode plate spacing and initial Pb(II) ions concentration on the electrosorption of Pb(II) ions were investigated, and the regenerative properties of graphene oxide electrodes were also investigated to provide an experimental basis for practical applications.

2. Materials and methods

2.1. Materials

Graphite powder (Qingdao Tianyuan Graphite Co., Ltd., China), H_2SO_4 (98%), $NaNO_3$ (99%), $KMnO_4$, H_2O_2 (30%), HCl (10%), Xylenol orange powder, anhydrous sodium acetate, glacial acetic acid.

2.2. Preparation of graphene oxide

In this experiment, the desired graphene oxide was synthesized by modified Hummers method. 2 g of graphite powder and 1 g of $NaNO_3$ were added to 46 mL of concentrated H_2SO_4 and treated by ultrasonic under ice bath conditions for 0.5 h. Then 8 g of $KMnO_4$ was added and stirred for 4 h under ice bath conditions. After that, the water bath temperature was adjusted to 40°C and ultrasonication was performed for 0.5 h. After adding 200 mL of deionized water and stirring well, the reaction was carried out in an oil bath at 95°C for 0.5 h. To terminate the reaction, 40 mL of deionized water and 10 mL of H_2O_2 were added to it. After stirring at low speed for 15 min, 40 mL of HCl was added to the mixture, and then the precipitate was repeatedly washed with deionized water in a high-speed centrifuge at a high speed of 9,000 rpm. After centrifugal washing, the product was dispersed in deionized water with the aid of ultrasound, which is a well-dispersed graphite oxide water dispersion. The product was dried in a vacuum oven at 60°C for 24 h to obtain graphite oxide.

2.3. Characterization of graphene oxide

In this experiment, the special functional groups of graphite powder and the graphene oxide were determined by Fourier-transform infrared spectroscopy (FT-IR; TENSOR27, Philips, Netherlands). The physical surface structures of the graphite and graphene oxide were determined by scanning electron microscopy (SEM; XL30, Bruker, Germany). The changes in the surface morphology of graphite and graphene oxide were measured by X-ray diffraction (XRD, X'Pert PRO, PANalytical, Netherlands).

2.4. Electrosorption experimental device and methods

The electrosorption device used in this experiment is shown in Fig. 1 and mainly consists of an electrosorption tank, a power supply controller and an electrosorption pole plate.

Experimental methods: Put the configured solution in the tank and insert the electrosorption electrode plate into the corresponding tank. The electrosorption experiments were carried out at the given voltage and plate spacing, and the solution samples were taken at regular intervals to analyze the concentration of Pb(II) ions and to calculate the adsorption capacity and removal efficiency of Pb(II) ions.

2.5. Analysis and test methods

2.5.1. Titration solution

0.01 mol/L EDTA standard solution. Add 3.72 g of disodium EDTA to 100 mL of deionized water, heat in a water bath until the drug is completely dissolved, leave to cool,

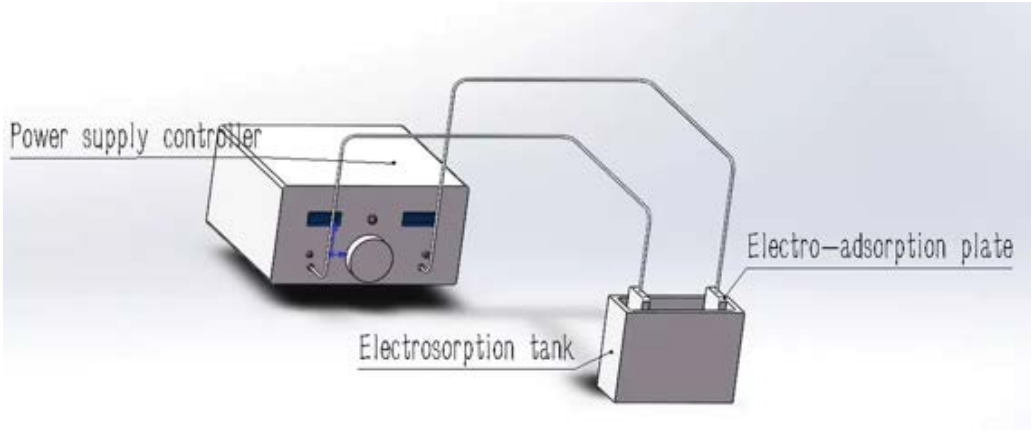

Fig. 1. Diagram of the electrosorption experimental device.

then pour into a 1,000 mL volumetric flask and dilute with deionized water to fix the volume.

2.5.2. Indicator

Xylenol orange aqueous solution with mass fraction of 0.2%. Dissolve 0.1 g of xylenol orange solid powder in a small amount of deionized water, and then dilute to a 50 mL volumetric flask.

2.5.3. Solution pH regulator

Add 150 g of anhydrous sodium acetate to 20 mL of glacial acetic acid, dilute with water to 200 mL, stir well, and use a 1,000 mL volumetric flask to dilute to volume.

2.5.4. Measurement method of Pb(II) ions concentration

Measure 25 mL of wastewater sample into a 250 mL conical flask, and adjust the pH of the solution to 5~6 with acetic acid-sodium acetate buffer. Add 2–3 drops of xylenol orange indicator to the conical flask to make the solution appear stable purple red. Then titrate with 0.01 mol/L standard EDTA solution until the solution changes from purple to bright yellow, and record the volume of EDTA used at this time. Calculate the Pb(II) ions concentration in solution by Eq. (1).

$$C = 207000 \times \frac{V \times 0.01}{25} \tag{1}$$

where C is the mass concentration of lead ions in the solution (mg/L), V is the volume of EDTA used in the titration (L).

The concentration of Pb(II) ions in the solution at different adsorption times was determined and the adsorption capacity at the electrode was calculated by Eq. (2).

$$Q = \frac{(C_0 - C)V}{m} \tag{2}$$

where Q is the capacity of electrosorption (mg/g), C is the concentration of Pb(II) ions in solution (mg/L), C_0 is the initial concentration of Pb(II) ions (mg/L), V is the volume of Pb(II) solution (L), m is the mass of graphene oxide (g).

2.6. Regenerative properties of graphene oxide electrode

After the electrosorption had reached equilibrium, the electrode was placed in a flow tank and rinsed with distilled water, and the power supply was reversed for the desorption time of 30 min. After the desorption was completed, the saturation adsorption of the graphene oxide electrode was measured and the regeneration efficiency of the graphene oxide electrode was calculated by Eq. (3).

$$\eta = \frac{Q_r}{Q_0} \tag{3}$$

where η is the regeneration efficiency, Q_0 and Q_t are the Pb(II) adsorption values of the graphite oxide electrode before and after the regeneration process respectively (mg/g).

3. Results and discussion

3.1. XRD analysis of graphene

Fig. 2 shows the XRD patterns of graphite and graphene oxide. From Fig. 2 it can be seen that graphite shows a more pronounced diffraction peak at 2θ = 26.5°, which corresponds to the characteristic reflection of the graphite (002) plane. In addition, the layer spacing of graphite was calculated by the Bragg equation to be 0.336 nm. In addition, a smaller but distinct diffraction peak appears at 2θ = 55°. However, graphene oxide shows a distinctive characteristic diffraction peak at 2θ = 10°, which corresponds to the characteristic reflection of the graphene oxide (001) plane. The layer spacing of graphene oxide was calculated from the Bragg equation to be 0.884 nm. The characteristic diffraction peak of graphene oxide is shifted in the direction of a small angle, indicating a lattice distortion of the carbon structure. The oxidation process incorporates a large number of oxygen-containing functional groups into the interlayer of graphite, which changes the intrinsic structure of graphite and allows the exfoliation of single atomic layers of graphite, increasing the specific surface area and adsorption sites of the material. The increased layer spacing of the graphene oxide sheet is due to the expansion of the graphene sheet and the presence of abundant oxygen-containing functional groups on both sides of the graphene sheet, resulting in atomic-level roughness on the graphene sheet.

3.2. Fourier transform infrared analysis of graphene oxide

The FT-IR spectra of graphite and graphene oxide are shown in Fig. 3. As can be seen from the figure, there is a broad and strong absorption peak near 3,445 cm^{-1}, which belongs to the stretching vibration peak of OH; at 1,632 cm^{-1} is the stretching vibration peak of C=O on the carboxyl group. The increase in intensity of this peak in graphene oxide confirms the formation of graphene oxide by oxidation of graphite. Compared with graphite, graphene oxide

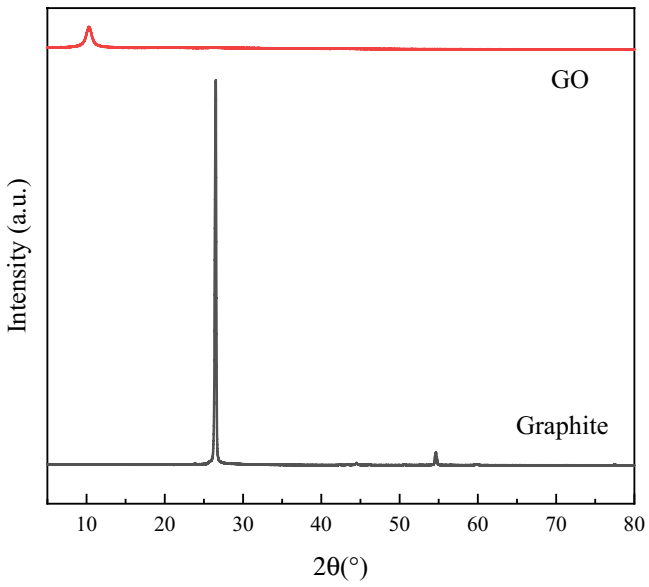

Fig. 2. XRD pattern of graphite and graphene oxide.

shows a vibrational absorption peak of C–O–C at 1,208 cm^{-1}; a vibrational absorption peak of C–O at 1,054 cm^{-1}, indicating that the oxidation treatment has increased its oxygen-containing functional groups. The oxidation process introduces a large number of functional groups on the graphite flake layer, resulting in a large number of oxygen-containing functional groups such as carboxyl, epoxy and hydroxyl groups on the surface of graphene oxide, increasing the number of active sites on the surface of graphene oxide. Table 1 lists characteristic absorption peaks and corresponding functional groups of graphene oxide. The changes of oxygen-containing functional groups before and after the adsorption of Pb(II) ions on graphene oxide were further analyzed by the FT-IR spectra. As shown in Fig. 3, the intensity of the peaks associated with oxygen-containing functional groups decreased significantly after the adsorption of Pb(II) ions by graphene oxide, where the intensity of the peaks associated with the hydroxyl and carbonyl groups decreased significantly and the peaks associated with the epoxy and carboxyl groups almost disappeared completely. This is mainly due to the ion-exchange and surface complexation between the Pb(II) ions and the oxygen-containing functional groups on the surface of the graphene oxide structure. The intensity of the peaks associated with the oxygen-containing functional groups is significantly reduced after the adsorption of Pb(II) ions by graphene oxide to form the corresponding complex GO- Pb(II). The above results indicate that the adsorption capacity of graphene oxide for Pb(II) ions mainly depends on the content of oxygen-containing functional groups on its surface.

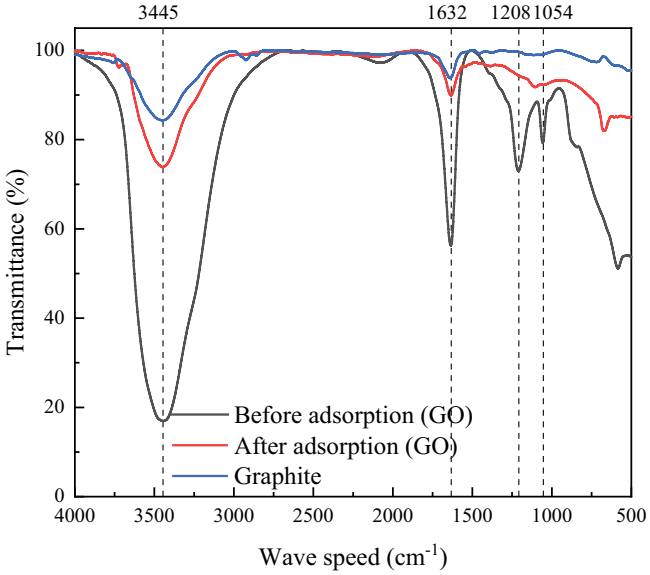

Fig. 3. FT-IR spectra of graphite and graphite oxide.

Table 1
Characteristic absorption peaks and corresponding functional groups of graphene oxide

Absorption peak position (cm^{-1})	Functional group
3,445	OH
1,632	C=O
1,208	C–O–C
1,054	C–OH

3.3. SEM analysis of graphite oxide

Fig. 4 shows SEM images of graphite and graphene oxide before and after adsorption. SEM image analysis shows that compared to graphite powder, graphite oxide exhibits a lamellar structure with a smoother surface and more folds at the edges. From Fig. 4e, it is clear that the graphite oxide lamellar structure is evident, with a multilayer folded flake surface. From Fig. 4f, it can be clearly seen that the edges of graphene oxide are stepped morphology or partially folded with a good layered structure. From the graph it can be analyzed that the oxidation process introduces a large number of oxygen-containing functional groups, which makes the graphene oxide layer structure obvious and increases the specific surface area, increasing the active sites on the surface of the graphene oxide. The SEM images before and after adsorption can be analyzed to show that the surface of graphene oxide after the adsorption of Pb(II) ions is rough and distributed with fine particles. This is mainly due to the ion-exchange and surface complexation between Pb(II) ions and oxygen-containing functional groups on the surface of the graphene oxide structure, forming the corresponding GO-Pb(II) complexes on the surface of the graphene oxide. The lamellar structure of the graphene oxide disappears and a rough flat block is formed on the surface. This is mainly due to the accumulation of the formed complexes on the graphene oxide surface, which changes the original lamellar structure of the graphene oxide.

3.4. Electrosorption experiments

3.4.1. Effect of different adsorbent materials

In order to express the good adsorption performance of graphene oxide in a more objective way, comparative analysis experiments were conducted with carbon fiber, activated carbon, and graphene oxide as adsorption materials, respectively. The relationship between adsorption capacity and adsorption time was investigated at the electrosorption voltage of 35 V, the positive and negative plate spacing of 1 cm and the initial solution concentration of 500 mg/L. The experimental results are shown in Fig. 5. The curve analysis showed that the adsorption capacity of the three adsorbents increased rapidly within the first 60 min, but the adsorption capacity of graphene oxide was much greater than that of activated carbon and carbon fiber. The graphene oxide synthesized in this study has a significant adsorption effect.

By analyzing the electrosorption curves of graphene oxide in Fig. 5, it can be seen that the adsorption process can be divided into three stages: fast adsorption (0–60 min), slow adsorption (60–120 min) and equilibrium adsorption (120–480 min) as the adsorption time increases. In the fast adsorption stage, the graphene oxide surface contains a large number of oxygen-containing functional groups, there are a large number of unoccupied active sites on the adsorbent surface, and the concentration gradient of Pb(II) ions in the solution and on the adsorbent surface is high,

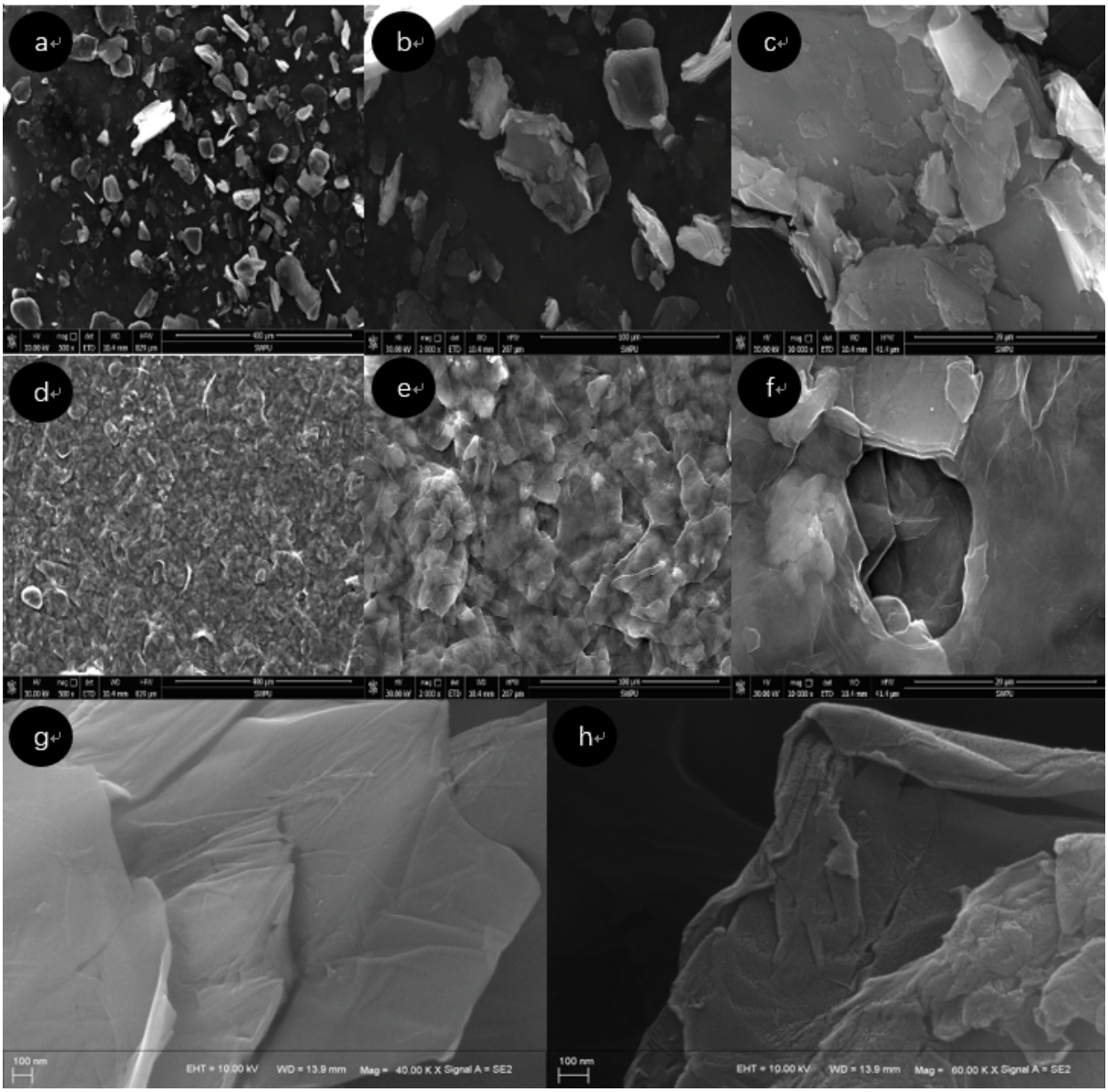

Fig. 4. SEM image of graphite/GO. (a) x500 graphite, (b) x2,000 graphite, (c) x10,000 graphite, (d) x500 GO, (e) x2000 GO, (f) x10,000 GO, graphene oxide before (g) and after (h) adsorption of Pb(II) ions.

which makes the rate of Pb(II) ions diffusion to the adsorbent surface faster, so the adsorption capacity increases rapidly. In the next stage, the adsorption rate slows down until it remains constant at the adsorption equilibrium state. This is due to the reduction of available active sites on the adsorbent surface and the reduced rate of diffusion of Pb(II) ions to the inner surface of the adsorbent.

To investigate the mechanism of Pb(II) ion adsorption by graphene oxide, the adsorption process at the graphite oxide electrode was fitted by the pseudo-first-order kinetic equation [Eq. (4)] and the pseudo-second-order kinetic equation [Eq. (5)].

$$Q_t = Q_e\left(1-\exp\left(-K_1 t\right)\right) \tag{4}$$

$$Q_t = \frac{Q_e^2 K_2 t}{1+Q_e K_2 t} \tag{5}$$

where t is the adsorption time (min), Q_t and Q_e are the capacity of adsorption at t and at equilibrium respectively (mg/g), K_1 and K_2 are the adsorption efficiency constants of pseudo-first and pseudo-second kinetics respectively (min^{-1}).

The fitted curves and their corresponding characteristic parameters are shown in Fig. 6 and Table 2, respectively. It can be seen that the R^2 of the pseudo-second-order kinetic fitting equation is significantly larger than that of the pseudo-first-order kinetic equation, and the adsorption process is in good agreement with the pseudo-second-order kinetic curve, indicating that the pseudo-second-order kinetic

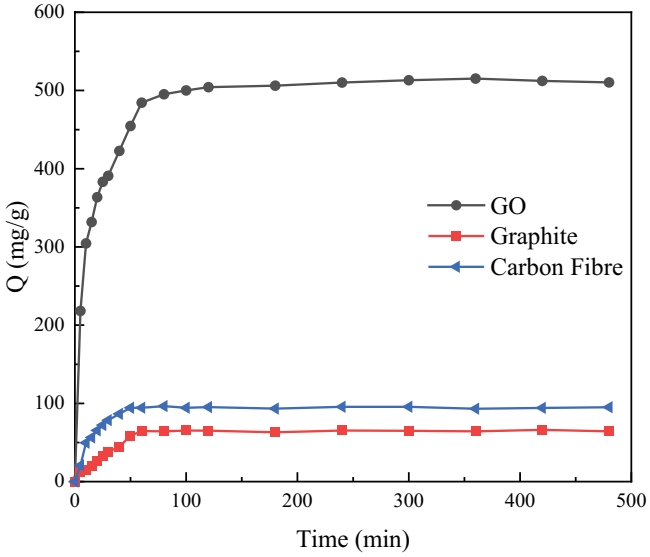

Fig. 5. Effect of different adsorbent materials.

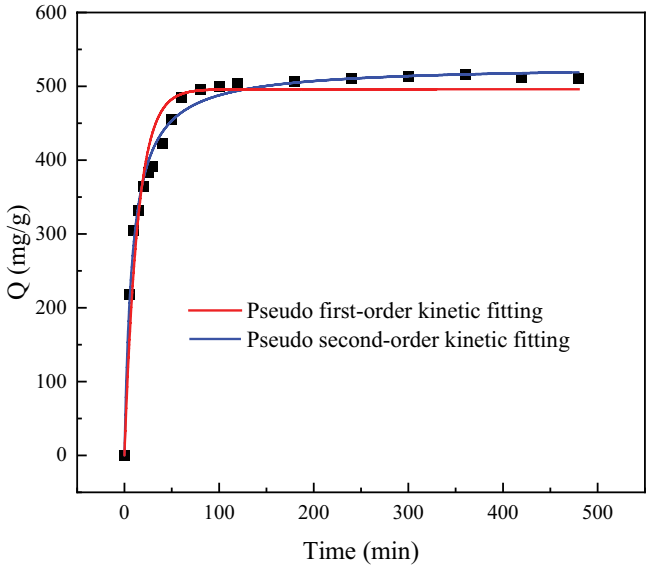

Fig. 6. Graphene oxide electrode electrosorption kinetic model fitting.

equation can be used to describe the electrosorption process at graphene oxide electrode. This indicates that the adsorption process of graphene oxide with Pb(II) ions is mainly affected by chemisorption. This may be due to the fact that graphene oxide contains many functional groups such as hydroxyl, carboxyl and carbonyl groups, and these active functional groups are able to adsorb Pb(II) ions through ion-exchange reactions and chemical bonding.

3.4.2. Effect of electrosorption voltage

The adsorption experiments with different voltages were investigated under the conditions of adsorption time of 60 min, plate spacing of 1 cm and Pb(II) ions concentration of 0.5 g/L. The experimental results are shown in Fig. 7. With

Table 2
Fitting parameters of pseudo-first-order and pseudo-second-order reaction kinetics

Electrode	Pseudo-first-order kinetics		Pseudo-second-order kinetics	
	K_1 (10^{-2} min^{-1})	R^2	K_2 (10^{-4} min^{-1})	R^2
GO	7.191	0.951	2.302	0.991

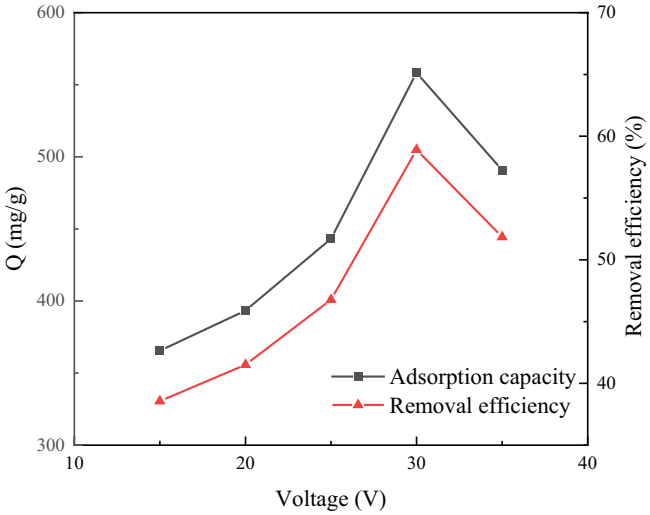

Fig. 7. Effect of electrosorption voltage.

the increase of adsorption voltage, the adsorption capacity and removal efficiency of Pb(II) ions increased gradually. When the adsorption voltage was 30 V, the adsorption capacity was 558.32 mg/g, and the removal efficiency of Pb(II) ions was 58.91%. Theoretically, the higher the voltage, the stronger the electrostatic field force, and the greater the efficiency and capability of electrosorption deionization. As the voltage increases, the attractive force of the provided electric field gradually increases, and the directional migration of ions in solution is enhanced by the electrostatic gravitational force. The increase in voltage also increases the thickness of the double layer formed, allowing more charged ions to be adsorbed. As a result the adsorption rate and the adsorption capacity increase, the adsorption effect increases and the removal rate also increases. When the adsorption voltage is greater than 30 V, electrolysis of water and electrode oxidation reactions occur in the solution and the current efficiency decreases, affecting the electrodes' electrosorption process. As a result, the adsorption rate and the adsorption capacity decrease, the adsorption effect decreases and the removal rate also decreases. And the higher voltage will increase the energy consumption and reduce the electrode life. According to the experimental results, the optimal adsorption voltage was determined to be 30 V.

3.4.3. Effect of plate spacing

The electrosorption experiments with different plate spacing were investigated under the conditions of

adsorption time of 60 min, adsorption voltage of 30 V and Pb(II) ions concentration of 0.5 g/L. The experimental results are shown in Fig. 8. The adsorption capacity and removal efficiency of Pb(II) ions increased gradually with the decrease of the plate spacing. At the plate spacing of 0.5 cm, the adsorption capacity was 620.21 mg/g, and the removal efficiency of Pb(II) ions was 65.42% at this time. According to the double layer theory, the thickness of the double layer formed on the electrodes has a large relationship with the electrode plate spacing. When the electrode plate spacing decreases, the double layer generated at the same electrode potential is thicker, so the adsorption capacity and adsorption effect will increase. Due to the increase in the thickness of the double electric layer, the graphene oxide was able to adsorb more Pb(II) ions on the original basis, thus increasing the removal rate of Pb(II) ions. However, too short the plate spacing can impede the flow of water and may short-circuit the electrode, increasing energy consumption. According to the experimental results, the optimum plate spacing was determined to be 0.5 cm.

3.4.4. Effect of the initial concentration of Pb(II) ions

The adsorption experiments with different initial concentrations were investigated under the experimental conditions of adsorption time of 60 min, adsorption voltage of 30 V and plate spacing of 0.5 cm. The experimental results are shown in Fig. 9. With the increase of the initial concentration, the adsorption capacity of Pb(II) ions increased gradually, but the removal efficiency of Pb(II) ions decreased continuously. This is because the concentration gradient of Pb(II) ions on the solution and adsorbent surface increases with increasing initial concentration, which makes the rate of Pb(II) ions diffusion to the adsorbent surface accelerate and the ion density around the electrode increase. Under the action of electric field, the contact between Pb(II) ions and the electrode increases, and the adsorption capacity and efficiency increases. However, as the initial concentration increases, the saturation adsorption capacity of the graphene oxide electrode remains unchanged, which makes the Pb(II) ion removal efficiency decrease and the treatment effect is reduced.

In order to investigate the maximum adsorption of Pb(II) ions by graphene oxide and further analyze its adsorption mechanism, the experimental data were fitted by Langmuir [Eq. (6)] and Freundlich [Eq. (7)] isothermal adsorption models. The fitted curves and their corresponding characteristic parameters are shown in Fig. 10 and Table 3.

$$Q_e = \frac{Q_m K_L C_e}{1 + K_L C_e} \tag{6}$$

$$Q_e = K_F C_e^{1/n} \tag{7}$$

where C_e is the concentration of Pb(II) ions in solution at equilibrium (mg/L), Q_e and Q_m are the equilibrium and

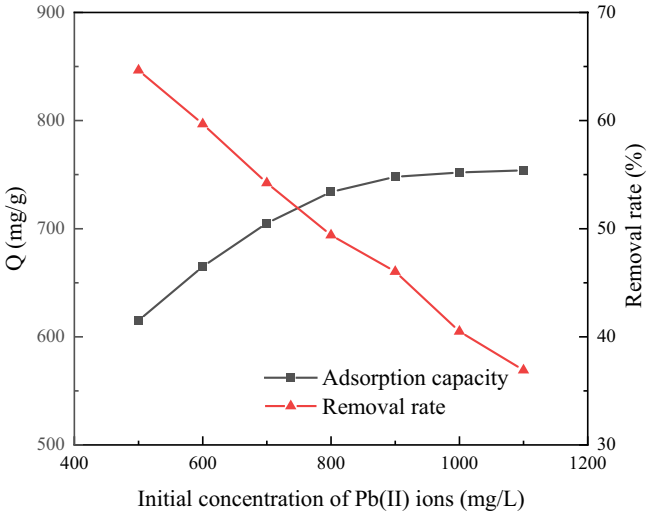

Fig. 9. Effect of the initial concentration of Pb(II) ions.

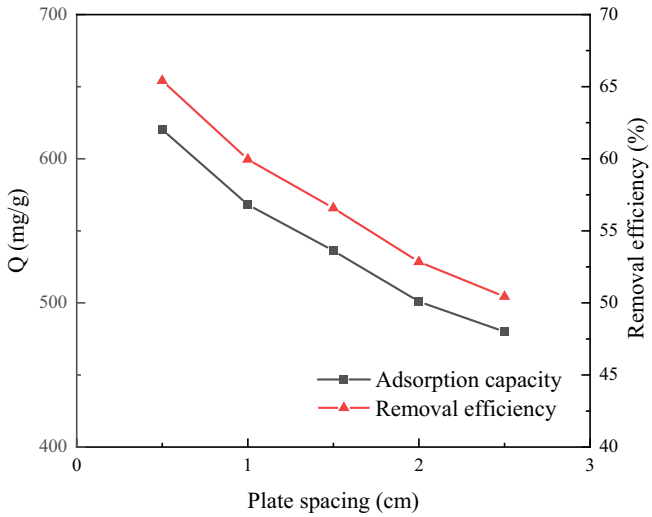

Fig. 8. Effect of plate spacing.

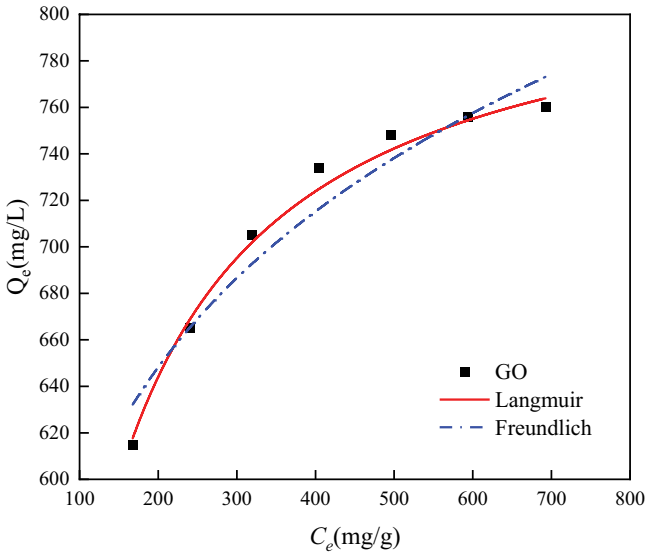

Fig. 10. Adsorption isotherms of Pb(II) ions by graphene oxide.

saturation sorption capacities respectively (mg/g), K_L and K_F are the Langmuir and Freundlich adsorption equilibrium constants respectively, n is the Freundlich constant related to the adsorption strength.

As shown in Fig. 10 and Table 3, the Langmuir model correlation coefficient (R^2 = 0.984) is significantly larger than that of the Freundlich model (R^2 = 0.925), indicating that the Langmuir model is more suitable for describing the electrosorption behaviour of graphene oxide on Pb(II) ions, and also indicating that its adsorption belongs to single molecular layer adsorption. The adsorption parameter 1/n is an important parameter to judge whether the adsorption occurs easily. Apparently, the adsorption parameter 1/n of graphene oxide on Pb(II) ions is about 0.15, which is less than 1, indicating that the electrosorption of Pb(II) ions by graphene oxide occurs easily. From the Langmuir model, the maximum adsorption of Pb(II) ions by graphene oxide reached 810.38 mg/g, this is more similar to the maximum adsorption of 760 mg/g measured under experimental conditions.

3.5. Regenerative properties of graphite oxide electrode

The great advantage of electrosorption is that the electrode is easily regenerated. By applying a reverse voltage to the electrode, the Pb(II) ions adsorbed on the electrode are returned to the solution by the reverse electric field, thus regenerating the electrode. Fig. 11 shows a graph of the regeneration efficiency of the graphene oxide electrode over 6 cycles. It can be seen from the graph that the regeneration rate for the first regeneration reached 75%. This indicates that there is physical adsorption on the electrode that cannot be completely desorbed, making the electrode not fully reusable. The subsequent regeneration rates were all around 72%, which shows the good recycling performance of the electrode.

Table 3
Fitting characteristic parameters for the adsorption isotherm equation

Electrode	Langmuir model			Freundlich model		
	K_L	Q_m	R^2	K_F	1/n	R^2
GO	0.018	810.38	0.984	305.64	0.15	0.925

4. Comparison with other studies

There are many other research methods for the removal of heavy metal ions such as ion-exchange, adsorption and bioremediation. The ion-exchange method (Liang et al. [25]; Golbad et al. [26]; Iqbal et al. [27]) for the removal of Pb(II) ions has the advantages of high removal rates, easy regeneration and effective recovery, but the disadvantages of the method are the high initial investment costs and the vulnerability of the ion-exchange agent to contamination or oxidation failure. The adsorption method (Hao et al. [28]; Hassan et al. [29]; Cataldo et al. [30]) has the advantages of high removal efficiency, low cost and simple operation, but it is limited by the low adsorption capacity and rate of the adsorbent and the high cost of regeneration. The bioremediation method (Sarı et al. [31]; Tüzün et al. [32]; Shanab et al. [33]) has the advantages of being environmentally friendly, low investment costs and no secondary pollution, but it has relatively strict requirements on the external environment and is unable to treat high concentrations of lead pollution,

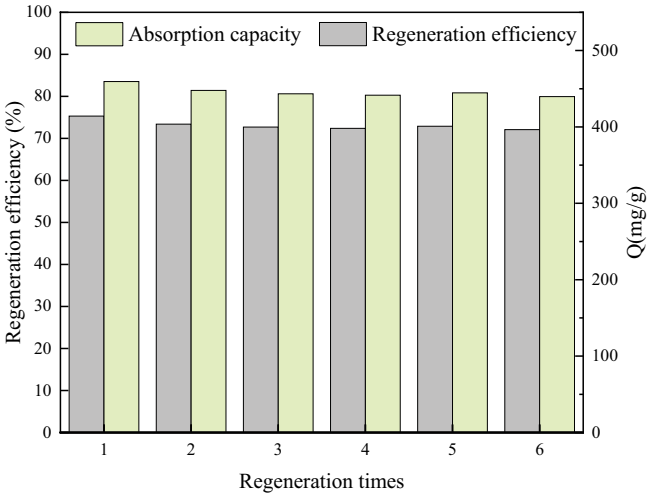

Fig. 11. Regeneration performance of graphene oxide electrode.

Table 4
Comparison of different adsorption methods for Pb(II) ion removal in other studies
From: The treatment of Pb(II) ions in wastewater by electrosorption

Adsorption method	Adsorbent	Q (mg/g)	References
Ion-exchange	MnO_2-biochar (MBR)	273	[25]
	Novel activated carbon-alginate composite	10.5	[26]
	Hydroxy sodalite	153.84	[27]
Adsorption	SiO_2/graphene composite	113.6	[28]
	TSGO	192.7	[29]
	Large-pore diameter nano-adsorbent	169.34	[30]
Bioremediation	Macrofungus (*Amanita rubescens*)	38.4	[31]
	Microalgae *Chlamydomonas reinhardtii*	93.8	[32]
	Green microalga *P. typicum*	5.51	[33]
Electroabsorption	Graphene oxide	627.02	This study

and the remediation cycle is affected by the growth of plants, making it difficult to achieve rapid remediation results. In this paper, the maximum adsorption capacity of the above adsorption methods were compared with this study and the data results are shown in Table 3. Compared with the other adsorption methods, the adsorption capacity of the electroabsorption method in this study are relatively high, and the adsorption rate and adsorption effect are better. Moreover, the method is simple to operate, environmentally friendly and low cost. Compared with other methods, the electroadsorption method has greater potential and feasibility for the removal of Pb(II) ions.

5. Conclusions

In this study, the layer spacing and specific surface area of graphene oxide synthesized by the modified Hummers method were increased to a certain extent, and a large number of oxygen-containing functional groups such as carbonyl, hydroxyl and carboxyl groups were present on the lamellae. The adsorption efficiency of Pb(II) ions was significantly increased by using graphite oxide as the electrode, and the adsorption process was in accordance with the pseudo-second-order kinetic equation. The effects of different parameters on electrosorption effect were investigated experimentally. The optimum conditions for the adsorption of graphene oxide electrode were the adsorption time of 60 min, the adsorption voltage of 30 V and the pole plate spacing of 0.5 cm. At this time, the adsorption capacity of the electrode was 627.02 mg/g and the removal efficiency of Pb(II) ions was 63.3%. With the increase of initial concentration, the adsorption capacity of Pb(II) ions by the electrode gradually increased, but the removal efficiency of Pb(II) ions continued to decrease and the treatment effect decreased. The regeneration performance of the graphene oxide electrode was good and stable, and the regeneration rate of the electrode was maintained at about 72% after several adsorption and regeneration cycles. This study provides an alternative way to treat heavy metal ions in wastewater without potential environmental problems and the electrodes can be reused, which is an applicable wastewater treatment technology.

References

[1] M.L. Mao, T.T. Yan, J.J. Shen, J.P. Zhang, D.S. Zhang, Capacitive removal of heavy metal ions from wastewater *via* an electro-adsorption and electro-reaction coupling process, Environ. Sci. Technol., 55 (2021) 3333–3340.

[2] H. Ucun, Y.K. Bayhan, Y. Kaya, A. Cakici, O.F. Algur, Biosorption of chromium(VI) from aqueous solution by cone biomass of *Pinus sylvestris*, Bioresour. Technol., 85 (2002) 155–158.

[3] X.B. Luo, L.L. Liu, F. Deng, S.L. Luo, Novel ion-imprinted polymer using crown ether as a functional monomer for selective removal of Pb(II) ions in real environmental water samples, J. Mater. Chem. A, 1 (2013) 8280–8286.

[4] Z.M. Khoshhesab, Z. Hooshyar, M. Sarfaraz, Removal of Pb(II) from aqueous solutions by NiO nanoparticles, Synth. React. Inorg. Met. -Org. Chem., 41 (2011) 1046–1051.

[5] Z. Chen, Y. Liang, D.S. Jia, W.Y. Chen, Z.M. Cui, X.K. Wang, Layered silicate RUB-15 for efficient removal of UO_2^{2+} and heavy metal ions by ion-exchange, Environ. Sci. Nano, 4 (2017) 1851–1858.

[6] D. Wang, Y.Y. Zuo, C.S. Qiu, N.N. Liu, C.C. Wang, S.P. Wang, J.J. Yu, L.P, Sun, Investigations on the biological treatment of mixed petrochemical industrial effluents based on acute toxicity and biodegradation characteristics, Desal. Water Treat., 179 (2020) 75–82.

[7] G.M. Ayoub, A. Hamzeh, L. Semerjian, Post treatment of tannery wastewater using lime/bittern coagulation and activated carbon adsorption, Desalination, 273 (2011) 359–365.

[8] T. Kim, J.E. Dykstra, S. Porada, A. van der Wal, J. Yoon, P.M. Biesheuvel, Enhanced charge efficiency and reduced energy use in capacitive deionization by increasing the discharge voltage, J. Colloid Interface Sci., 446 (2015) 317–326.

[9] N. Lesage, M. Sperandio, C. Cabassud, Study of a hybrid process: adsorption on activated carbon/membrane bioreactor for the treatment of an industrial wastewater, Chem. Eng. Process., 47 (2008) 303–307.

[10] C.Y. Zhang, L. Wu, J.X. Ma, A. Ninh Pham, M. Wang, T. David Waite, Integrated flow-electrode capacitive deionization and microfiltration system for continuous and energy-efficient brackish water desalination, Environ. Sci. Technol., 53 (2019) 13364–13373.

[11] P. Srimuk, X. Su, J.Y. Yoon, D. Aurbach, V. Presser, Charge-transfer materials for electrochemical water desalination, ion separation and the recovery of elements, Nat. Rev. Mater., 5 (2020) 517–538.

[12] X.D. Zhang, K.C. Zuo, X.R. Zhang, C.Y. Zhang, P. Liang, Selective ion separation by capacitive deionization (CDI) based technologies: a state-of-the-art review, Environ. Sci. Water Res. Technol., 6 (2020) 243–257.

[13] X.J. Ma, Y. Gao, Y. Cui, H.P. Huang, J.Y. Han, Electrochemical treatment of papermaking tobacco sheet wastewater on β-PbO_2 and Ti/TiO_2-RuO_2-IrO_2 electrodes, Desal. Water Treat., 57 (2016) 19557–19565.

[14] Z. Huang, L. Lu, Z.X. Cai, Z.J. Jason Ren, Individual and competitive removal of heavy metals using capacitive deionization, J. Hazard. Mater., 302 (2016) 323–331.

[15] R.L. Chen, T. Sheehan, J.L. Ng, M. Brucks, X. Su, Capacitive deionization and electrosorption for heavy metal removal, Environ. Sci. Water Res. Technol., 6 (2020) 258–282.

[16] G.Z. Wang, T.T. Yan, J.P. Zhang, L.Y. Shi, D.S. Zhang, Trace-Fe-enhanced capacitive deionization of saline water by boosting electron transfer of electro-adsorption sites, Environ. Sci. Technol., 54 (2020) 8411–8419.

[17] H. Wang, T.T. Yan, J.J. Shen, J.P. Zhang, L.Y. Shi, D.S. Zhang, Efficient removal of metal ions by capacitive deionization with straw waste derived graphitic porous carbon nanosheets, Environ. Sci. Nano, 7 (2020) 317–326.

[18] H. Grajek, J. Jonik, Z. Witkiewicz, T. Wawer, M. Purchala, Applications of graphene and its derivatives in chemical analysis, Crit. Rev. Anal. Chem., 50 (2020) 445–471.

[19] R.K. Singh, R. Kumar, D.P. Singh, Graphene oxide: strategies for synthesis, reduction and frontier applications, RSC Adv., 6 (2016) 64993–65011.

[20] Y. Wang, S.S. Li, H.Y. Yang, J. Luo, Progress in the functional modification of graphene/graphene oxide: a review, RSC Adv., 10 (2020) 15328–15345.

[21] H.B. Li, L.D. Zou, L.K. Pan, Z. Sun, Novel graphene-like electrodes for capacitive deionization, Environ. Sci. Technol., 44 (2010) 8692–8697.

[22] A.G. El-Deen, N.A.M. Barakat, K.A. Khalil, M. Motlak, H.Y. Kim, Graphene/SnO_2 nanocomposite as an effective electrode material for saline water desalination using capacitive deionization, Ceram. Int., 40 (2014) 14627–14634.

[23] B.K. Ong, H.L. Poh, C.K. Chua, M. Pumera, Graphenes prepared by Hummers, Staudenmaier and Hofmann methods for analysis of TNT-based nitroaromatic explosives in seawater, Electroanalysis, 24 (2012) 2085–2093.

[24] S.T. Xu, J.K. Liu, Y. Xue, T.Y. Wu, Z.F. Zhang, Appropriate conditions for preparing few-layered graphene oxide and reduced graphene oxide, Fullerenes Nanotubes Carbon Nanostruct., 25 (2017) 40–46.

[25] J. Liang, X. Li, Z. Yu, G. Zeng, Y. Luo, L. Jiang, Z. Yang, Y. Qian, H. Wu, Amorphous MnO_2 modified biochar derived from aerobically composted swine manure for adsorption of Pb(II) and Cd(II), ACS Sustainable Chem. Eng., 5 (2017) 5049–5058.

[26] S. Cataldo, A. Gianguzza, D. Milea, N. Muratore, A. Pettignano, Pb(II) adsorption by a *novel* activated carbon – alginate composite material. A kinetic and equilibrium study, Int. J. Biol. Macromol., 92 (2016) 769–778.
[27] S. Golbad, P. Khoshnoud, N. Abu-Zahra, Hydrothermal synthesis of hydroxy sodalite from fly ash for the removal of lead ions from water, Int. J. Environ. Sci. Technol., 14 (2017) 135–142.
[28] L.Y. Hao, H. Song, L.C. Zhang, X.Y. Wan, Y.R. Tang, Y. Lv, SiO_2/graphene composite for highly selective adsorption of Pb(II) ion, J. Colloid Interface Sci., 369 (2012) 381–387.
[29] A.F. Hassan, R. Bulánek, Preparation and characterization of thiosemicarbazide functionalized graphene oxide as nanoadsorbent sheets for removal of lead cations, Int. J. Environ. Sci. Technol., 16 (2019) 6207–6216.
[30] A. Shahat, Md.R. Awual, Md.A. Khaleque, Md.Z. Alam, Mu. Naushad, A.M.S. Chowdhury, Large-pore diameter nano-adsorbent and its application for rapid lead(II) detection and removal from aqueous media, Chem. Eng. J., 273 (2015) 286–295.
[31] A. Sarı, M. Tuzen, Kinetic and equilibrium studies of biosorption of Pb(II) and Cd(II) from aqueous solution by macrofungus (*Amanita rubescens*) biomass, J. Hazard. Mater., 164 (2009) 1004–1011.
[32] İ. Tüzün, G. Bayramoğlu, E. Yalçın, G. Başaran, G. Çelik, M. Yakup Arıca, Equilibrium and kinetic studies on biosorption of Hg(II), Cd(II) and Pb(II) ions onto microalgae *Chlamydomonas reinhardtii*, J. Environ. Manage., 77 (2005) 85–92.
[33] S. Shanab, A. Essa, E. Shalaby, Bioremoval capacity of three heavy metals by some microalgae species (Egyptian Isolates), Plant Signaling Behav., 7 (2012) 392–399.